Article

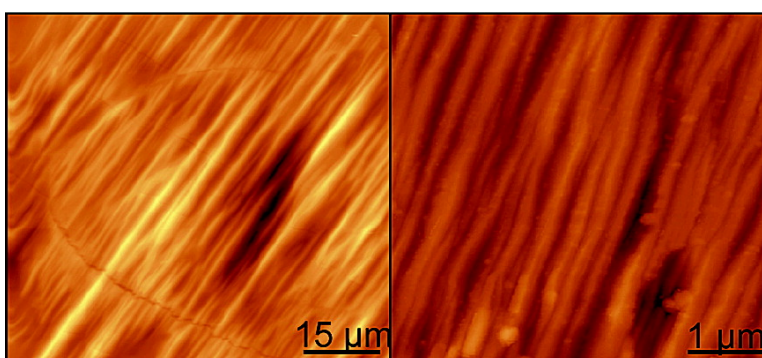# Multiscale Self-Organization of the Organic Semiconductor α-Quinquethiophene

Manuela Melucci, Massimo Gazzano, Giovanna Barbarella, Massimiliano Cavallini, Fabio Biscarini, Piera Maccagnani, and Paolo Ostoja

More About This Article

Additional resources and features associated with this article are available within the HTML version:

- Supporting Information
- Links to the 11 articles that cite this article, as of the time of this article download
- Access to high resolution figures
- Links to articles and content related to this article
- Copyright permission to reproduce figures and/or text from this article

View the Full Text HTML

Multiscale Self-Organization of the Organic Semiconductor α-Quinquethiophene

Manuela Melucci,[†] Massimo Gazzano,[†] Giovanna Barbarella,*,[†]
Massimiliano Cavallini,[‡] Fabio Biscarini,[‡] Piera Maccagnani,[§] and Paolo Ostoja[§]

*Contribution from the Istituto per la Sintesi Organica e la Fotoreattivita' (ISOF), Istituto per i
Materiali Nanostrutturati (ISMN), and Istituto per la Microelettronica e i Microsistemi (IMM),
Consiglio Nazionale delle Ricerche, Via Gobetti 101, 40129 Bologna, Italy*

Received May 14, 2003; E-mail: barbarella@isof.cnr.it

Abstract: We show that thin films grown by vacuum sublimation, or formed by melted powders, of semiconductor α-quinquethiophene (T5) exhibit a hierarchical self-affinity organization that spans scales from tens of nanometers to hundreds of micrometers. T5 organization was investigated by X-ray diffraction (XRD), atomic force microscopy (AFM), and optical microscopy. XRD showed that vacuum-evaporated T5 films were characterized by a preferred orientation of the *h*00 planes parallel to the glass substrate. Melting of the films followed by rapid quenching to room temperature led to the formation of micrometer-sized, single-crystal-like structures, characterized by uniaxially aligned stripes. XRD proved that the melting− quenching process enhanced molecular ordering and increased the size of domains with the molecule's long axes tilted by about 65° with respect to the substrate plane and piled up side-by-side along parallel columns. AFM measurements on the melt-quenched structures showed that a hierarchical architecture was built by reiteration across multiple length scales of the same recurring motif. Because of the tendency of T5 to form highly crystalline vacuum-evaporated thin films, a field-effect hole mobility comparable to state-of-the-art FET mobility of α-sexithiophene films was reached, without any attempt to optimize deposition conditions.

Numerous studies published on thiophene oligomers in the past decade[1] have been prompted by the potential use of these compounds in organic-based electronics, in particular, thin film field-effect transistors.[2−4] The technology of organic thin film transistors (OTFTs) is expected to compete soon with the technology of hydrogenated amorphous silicon, and thiophene oligomers are among the best semiconductor molecular materials that have been investigated.[4]

There are many open questions about semiconductor conjugated materials as electric charge carriers, but it is a consolidated opinion that high structural ordering is a necessary, although not sufficient, condition for achieving large charge carrier mobilities required for technologically attractive device applications.[2−4] The coherence length of the crystalline domains formed by these compounds in thin films (typically 10−100 nm) is not the only relevant length scale, but also correlation lengths that characterize the thin film morphology become extremely important and need to be understood and controlled. How to control on the same footings the molecular ordering, which depends on weak interactions, and the morphology, which is governed by the mechanism of growth, is not trivial. A challenging problem is to find suitable materials and processing strategies able to yield ordered, organized architectures across the length scales connecting the molecules to the device structure.

Thiophene oligomers can be regarded as one of the richest and more versatile systems for building organized structures across multiple length scales. They exhibit a variety of intra- and intermolecular interactions[5] − van der Waals interactions, weak hydrogen bondings, π−π stacking, sulfur−sulfur interactions − all related to the "plasticity" of the thiophene ring,[6a] originating from the high polarizability of sulfur electrons. The "plasticity" of the thiophene ring, that is, the ability to adapt to

† ISOF.
‡ ISMN.
§ IMM.

(1) (a) Fichou, D. *J. Mater. Chem.* **2000**, *10*, 571−588. (b) Fichou, D., Ed.; *Handbook of oligo and polythiophenes*; Wiley-VCH: New York, 1999. (c) Müllen, K., Wegner, G., Eds. *Electronic Materials: The Oligomer Approach*; Wiley-VCH: New York, 1998. (d) Nalwa, H. S., Ed. *Handbook of Organic Conductive Molecules and Polymers*; J. Wiley & Sons: Chichester, 1997.

(2) (a) Garnier, F. *Acc. Chem. Res.* **1999**, *32*, 209−215. (b) Hajlaoui, R.; Horowitz, G.; Garnier, F.; Arce-Brouchet, A.; Laigre, L.; El Kassmi, A.; Demanze, F.; Kouki, F. A*dv. Mater.* **1997**, *9*, 389−391. (c) Horowitz, G.; Fichou, D.; Peng, X. Z.; Xu, Z. G.; Garnier, F. *Solid State Commun.* **1989**, *72*, 381−383. (d) Horowitz, G.; Garnier, F.; Yassar, A.; Hajlaoui, R.; Kouki, F. A*dv. Mater.* **1996**, *8*, 52−54. (e) Garnier, F.; Yassar, A.; Hajlaoui, R.; Horowitz, G.; Deloffre, F.; Servet, B.; Ries, S.; Alnot, P. *J. Am. Chem. Soc.* **1993**, *115*, 8716−8721.

(3) (a) Katz, H. E.; Bao, Z. N.; Gilat, S. L. *Acc. Chem. Res.* **2001**, *34*, 359−369. (b) Katz, H. E.; Lovinger, A. J.; Laquindanum, J. G. *Chem. Mater.* **1998**, *10*, 457−459. (c) Laquindanum, J. G.; Katz, H. E.; Lovinger, A. J. *J. Am. Chem. Soc.* **1998**, *120*, 664. (d) Katz, H. E. *J. Mater. Chem.* **1997**, *7*, 369−376. (e) Torsi, L.; Dodabalapur, A.; Rothberg, L. J.; Fung, A. W. P.; Katz, H. E. *Science* **1996**, *272*, 1462−1464. (f) Lovinger, A. J.; Davis, D. D.; Dodabalapur, A.; Katz, H. E.; Torsi, L. *Macromolecules* **1996**, *29*, 4952−4957. (g) Dodalabapur, A.; Torsi, L.; Katz, H. E. *Science* **1995**, *268*, 270−271.

(4) Dimitrakopoulos, C. D.; Malenfant, P. R. L. *Adv. Mater.* **2002**, *14*, 99−117.

(5) Marseglia, E. A.; Grepioni, F.; Tedesco, E.; Braga, D. *Mol. Cryst. Liq. Cryst.* **2000**, *348*, 137−151.

the environment by ease of deformation of the bond angle and length, gives rise to a variety of conformations and packing motifs in the solid state, which are fascinating but unpredictable at the present state of knowledge. Conformational polymorphism leads to different packing types for the same molecule and different optical properties for the bulk material.[6b,c] Much has been learned about the self-organization properties of thiophene oligomers from single-crystal and powder X-ray diffraction data.[5,7,8] Among unsubstituted thiophene oligomers, single-crystal X-ray data have been reported for α-ter-,[9] quater-,[10] sexi-,[11] and octithiophene.[12] Thus, the great majority of the data reported on the solid-state supramolecular organization of unsubstituted oligothiophenes concerns even term compounds.

The most studied thiophene oligomer is α-sexithiophene (T6), which is a liquid crystalline compound and exhibits spontaneously long-range molecular order.[6d,13] T6, however, is insoluble, and this makes achieving a high purity standard for electronic applications difficult. This is partly responsible for the slow increase, over the years, of T6 charge mobility since the discovery of its semiconducting properties.[2c,d] T6 films grown by high vacuum sublimation exhibit a variety of morphologies that are due to different dominant mechanisms of growth and affect charge mobility.[14] Ordered films can only be grown at high substrate temperatures, small thicknesses, and low deposition rates.[8c,14]

The shorter homologue of T6, α-quinquethiophene T5, has been much less studied. T5 is more difficult to synthesize than T6, but has the advantage of being slightly soluble in a few organic solvents which makes it easier to purify. At the same time, solubility offers the possibility of processing thin films by solution deposition or casting, which are more relevant in view of large area applications. By an improvement in synthetic methodologies using microwave-assisted[15] Suzuki coupling, we have been able recently to obtain highly pure thiophene oligomers, including T5.[6f] Starting from halogenated building blocks of different size, we were able to obtain thiophene oligomers rapidly and in good yields, which could be purified by sublimation using a coldfinger.

Neither single-crystal structure nor thin film X-ray diffraction data have been reported for T5. Scarce data from different laboratories on field-effect charge mobility — generally quoted between 1 and 2 orders of magnitude below that of T6 — have been published.[2b,16] Interestingly, experimental data obtained by a variety of structural techniques strongly suggest that T5 can self-organize into layered structures,[17] which makes it promising as an organic semiconductor with high charge carrier mobility.
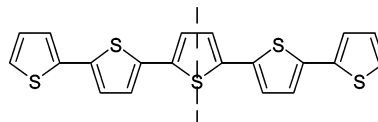
T5

The odd number of thiophene rings of T5 makes its molecular symmetry different from that of the even-term oligomers. This, together with the presence of a permanent dipole, may produce different supramolecular architectures with respect to even-term compounds. An indication in this direction comes from the comparison of solid-state ^{13}C NMR spectra of α-ter- and quinquethiophene with those of α-quarter and sexithiophene.[6e] However, according to X-ray powder diffraction data, odd- and even-term unsubstituted oligothiophenes are characterized by common structural features, with very similar packing arrangements.[7] Thus, it is important to investigate the organization of odd- and even-term oligomers at different length scales, viz., morphology and scaling behavior.

In this paper, we show that T5 films obtained by a simple melting—quenching procedure exhibit an enhanced crystal order together with a remarkable self-affine morphology, spanning length scales from tens of nanometers to hundreds of micrometers as observed by X-ray diffraction, atomic force microscopy, and optical microscopy. We also show that T5 films yield hole mobilities on the order of 0.02 cm^2/(V·s) that compare to T6 thin film FET mobility. These results strongly suggest that the hierarchical structure, spontaneously present in T5, is a key ingredient in achieving high mobility organic semiconductors.

Results

I. Thermal Behavior and Optical Observations. The differential scanning calorimetry (DSC) plot of T5, carried out at a scanning rate of 10 °C min^{-1} for both heating and cooling cycles, is shown in Figure 1. The same plot was obtained using a scanning rate of 2 °C min^{-1}.

(6) (a) Barbarella, G.; Zambianchi, M.; Bongini, A.; Antolini, L. *Adv. Mater.* **1993**, *5*, 834–838. (b) Barbarella, G.; Zambianchi, M.; Marimon del Fresno, M.; Antolini, L.; Bongini, A. *Adv. Mater.* **1997**, *9*, 484–487. (c) Barbarella, G.; Zambianchi, M.; Antolini, L.; Ostoja, P.; Maccagnani, P.; Bongini, A.; Marseglia, E. A.; Tedesco, E.; Gigli, G.; Cingolani, R. *J. Am. Chem. Soc.* **1999**, *121*, 1, 8920–8926. (d) Scandola, M.; Finelli, L.; Bongini, A.; Barbarella, G.; Sotgiu, G.; Zambianchi, M. *Macromol. Chem. Phys.* **2001**, *202*, 1878–1882. (e) Barbarella, G.; Casarini, D.; Zambianchi, M.; Favaretto, L.; Rossini, S. *Adv. Mater.* **1996**, *8*, 69–73. (f) Melucci, M.; Barbarella, G.; Sotgiu, G. *J. Org. Chem.* **2002**, *67*, 8877–8884.
(7) Porzio, W.; Destri, S.; Mascherpa, M.; Brückner, S. *Acta Polym.* **1993**, *44*, 266–272.
(8) (a) Ostoja, P.; Guerri, S.; Rossini, S.; Servidori, M.; Taliani, C.; Zamboni, C. R. *Synth. Met.* **1993**, *54*, 447–452. (b) Lovinger, A. J.; Davis, D. D.; Dodalabapur, A.; Katz, H. E. *Chem. Mater.* **1996**, *8*, 2836–2838. (c) Servet, B.; Horowitz, G.; Ries, S.; Lagorsse, O.; Alnot, P.; Yassar, A.; Deloffre, F.; Srivastava, P.; Hajlaoui, R.; Lang, P.; Garnier, F. *Chem. Mater.* **1994**, *6*, 1809–1815.
(9) van Bolhuis, F.; Wynberg, H.; Havinga, E. E.; Meijer, E. W.; Staring, E. G. J. *Synth. Met.* **1989**, *30*, 381–389.
(10) (a) Antolini, L.; Horowitz, G.; Kouki, F.; Garnier, F. *Adv. Mater.* **1998**, *10*, 382–385. (b) Siegrist, T.; Kloc, C.; Laudise, R. A.; Katz, H. E.; Haddon, R. C. *Adv. Mater.* **1998**, *10*, 379–382.
(11) (a) Horowitz, G.; Bachet, B.; Yassar, A.; Lang, P.; Demanze, F.; Fave, J. L.; Garnier, F. *Chem. Mater.* **1995**, *7*, 1337–1341. (b) Siegrist, T.; Fleming, R. M.; Haddon, R. C.; Laudise, R. A.; Lovinger, A. J.; Katz, H. E.; Bridenbaugh, P.; Davis, D. D. *J. Mater. Res.* **1995**, *10*, 2170–2173.
(12) Fichou, D.; Bachet, B.; Demanze, F.; Billy, I.; Horowitz, G.; Garnier, F. *Adv. Mater.* **1996**, *8*, 500–504.
(13) Taliani, C.; Zamboni, R.; Ruani, G.; Rossini, S.; Lazzaroni, R. *J. Mol. Electron.* **1990**, *6*, 225–226.
(14) (a) Biscarini, F.; Zamboni, R.; Samori, P.; Ostoja, P.; Taliani, C. *Phys. Rev. B* **1995**, *52*, 14868–14877. (b) Biscarini, F.; Samori, P.; Greco, O.; Zamboni, R. *Phys. Rev. Lett.* **1997**, *78*, 2389–2392. (c) Viville, P.; Lazzaroni, R.; Brédas, J. L.; Moretti, P.; Samorí, P.; Biscarini, F. *Adv. Mater.* **1998**, *10*, 57–60.
(15) Adam, D. *Nature* **2003**, *421*, 571–572.
(16) Hong, X. M.; Katz, H. E.; Lovinger, A. J.; Wang, B. C.; Raghavachari, K. *Chem. Mater.* **2001**, *13*, 4686–4691.
(17) (a) Muller, E.; Ziegler, C. *J. Mater. Chem.* **2000**, *10*, 47–53. (b) Pellegrino, O.; Vilar, M. R.; Horowitz, G.; Kouki, F.; Garnier, F.; da Silva, J. D. L.; doRego, A. M. B. *Thin Solid Films* **1998**, *327*, 252–255. (c) Kramer, M.; Hoffmann, V. *Opt. Mater.* **1998**, *9*, 65–69. (d) Pal, A. J.; Osterbacka, R.; Kallman, K. M.; Stubb, H. *Appl. Phys. Lett.* **1997**, *71*, 228–230. (e) Isz, S.; Weissbuch, I.; Kjaer, K.; Bouwman, W. G.; Als-Nielsen, J.; Palacin, S.; Ruaudel-Teixier, A.; Leiserowitz, L.; Lahav, M. *Chem.-Eur. J.* **1997**, *3*, 930–939. (f) Soukopp, A.; Glöckler, K.; Bäuerle, P.; Sokolowski, M.; Umbach, E. *Adv. Mater.* **1996**, *8*, 902–906. (g) Böhme, O.; Ziegler, C.; Göpel, W. *Adv. Mater.* **1994**, *6*, 587–590. (h) Hotta, S.; Waragai, K. *Adv. Mater.* **1993**, *5*, 896–908.
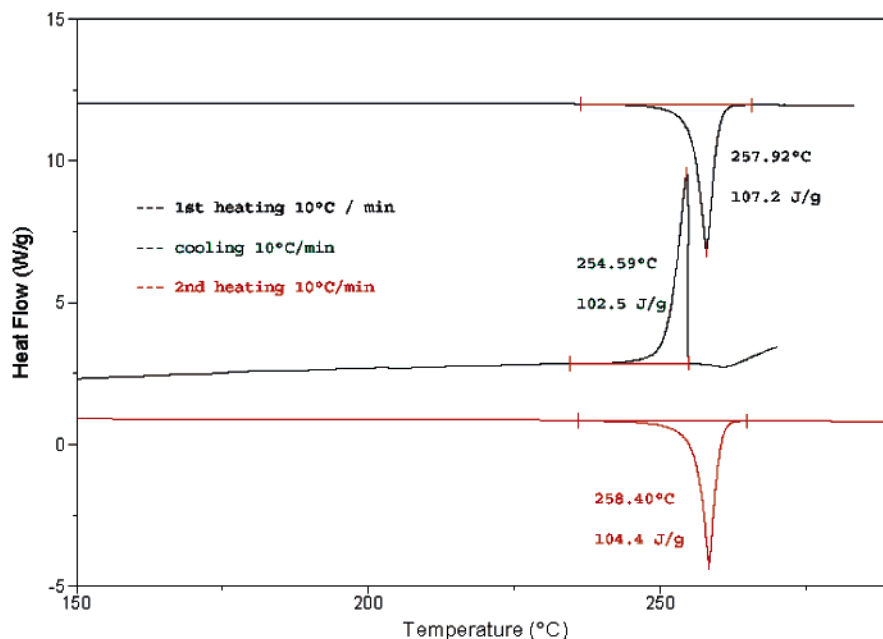
Figure 1. Differential scanning calorimetry of T5 at a scanning rate of 10 °C min^{-1} for heating and cooling cycles.
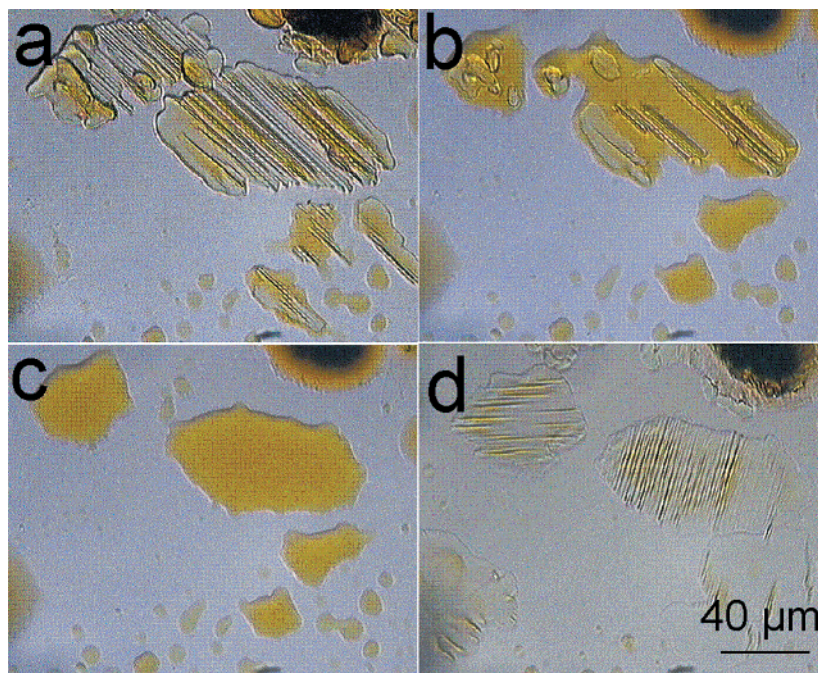

Figure 2. Optical micrographs (parallel polarizers) of melt-quenched T5 powder. (a) After the first melting–quenching cycle. (b,c) Melting. (d) After the second thermal quenching.

DSC scans exhibit only the crystallization peaks (255–258 °C). No evidence of formation of a smectic liquid-crystalline phase was found, contrary to expectations based on early studies.[17c] In the same experimental conditions, the DSC plot of T6 showed two endothermal peaks, which were attributed to meso-phase formation and isotropization,[6d] and optical microscopy showed the presence of the Schlieren texture typical of nematic liquid crystals.[13]

In agreement with DSC data, no evidence of liquid crystalline phases was found by optical microscopy observations. However, we found that melting of T5 powder at $T \approx 250$ °C followed by rapid thermal quenching to ambient temperature led to a morphology reorganization, with the appearance of uniaxially

aligned microsized stripes in the recrystallized sample. The formation of the stripes was reversible, as they always formed in repeated melting–quenching cycles. However, the orientation of the stripes changed with respect to the isotropic glass substrate from one cycle to the other, indicating random nucleation (Figure 2).

The same phenomenology was consistently observed in thin films of different thickness, either high vacuum-evaporated or spin-coated, provided the temperature was allowed to drop rapidly after melting had occurred. Because T5 tends to sublime at temperatures close to the melting point, the melting–quenching process was performed on thin films covered with a glass slip. The melting of the films led to the formation of
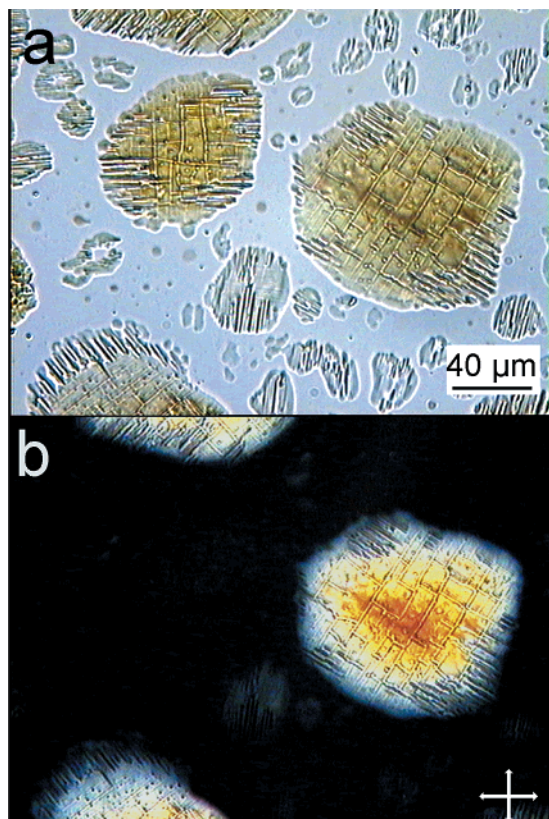
Figure 3. Optical micrographs of T5 on glass after a single melting−quenching cycle. (a) Micrographs taken under unpolarized light. (b) Micrographs taken between crossed polars oriented along the axis of the image. The crystals are extinguished when the crossed polars are oriented parallel or perpendicular to the stripes and are brightest at 45°.

microscopic droplets, hundreds of micrometers in diameter, which after thermal quenching exhibited stripes similar to those shown in Figure 2 and which were reversibly formed upon repeating melting−quenching cycles without any memory effect of previous orientations.

Vacuum-evaporated 100−200 nm thick films displayed an intense XRD pattern after the melting−quenching process (see section III), while spin-coated films were too thin for XRD analysis.

As a term of comparison, attempts to obtain similar crystalline structures by melting−quenching of T6 were unsuccessful.

II. Morphology. The samples of T5 prepared on glass by the melting−quenching process were investigated by polarized optical microscopy and atomic force microscopy (AFM).

As shown in the optical micrograph of Figure 3 (top), the samples exhibit the presence of large crystallites formed as soon as the melted T5 was thermally quenched. The crystal size ranges from a few micrometers to hundreds of micrometers. No evidence of the liquid crystalline phase was observed by cross polars before the melted T5 became solid. The shape of the domains is irregular and does not hint at a specific crystal order. Under illumination with nonpolarized light, the crystals appears to be strongly colored yellow, the same color as the powder. All crystals exhibit a texture of parallel stripes across their surfaces. However, no correlation between the orientation of the stripes among different crystals has been observed.

The largest crystals exhibited fracture lines due to thermal stress, which occurred during the quenching. These fractures are not visible in smaller crystals with the resolution of the optical microscope. We estimated the critical dimension for the appearance of fractures to be around 40 μm in diameter. The fracture lines were either parallel or perpendicular to the stripes.

The observation with crossed polars (Figure 3 bottom) showed the typical behavior of optically anisotropic materials: the background does not transmit light, while the crystals appear colored under crossed polars, with colors ranging from violet to yellow depending on the local thickness. Rotation of the microscope stage (viz., the crystal orientation vs the polarized light) led to the crystals being extinguished (became dark) in four positions at intervals of 90° when the crossed polars were oriented parallel (perpendicular) to the stripes (see the video reported as Supporting Information). The evidence of light extinction at the same orientations in all crystals indicates that the domains within each crystal have the same orientation.

The melted-quenched thin films were investigated by AFM operating in noncontact mode. As shown in Figure 4, the film morphology is characterized by striped domains even at length scales substantially smaller that the ones accessible to the optical microscope. It is clear from Figure 4a and 4b that a similar morphology is retained upon a change of the spatial scale of observation of more than 1 order of magnitude. The quantitative matching of a morphology onto another at different length scales requires anisotropic scaling of the topography height. This type
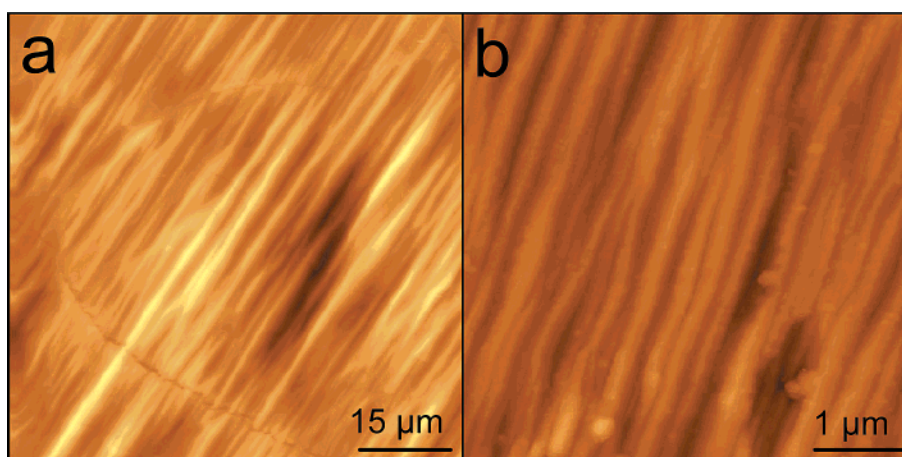

Figure 4. AFM images of T5 on glass after the melting−quenching cycle. The two images show the similarity in morphology at different magnifications. (a) Height range z: 0−940 nm. (b) Height range z: 0−370 nm.
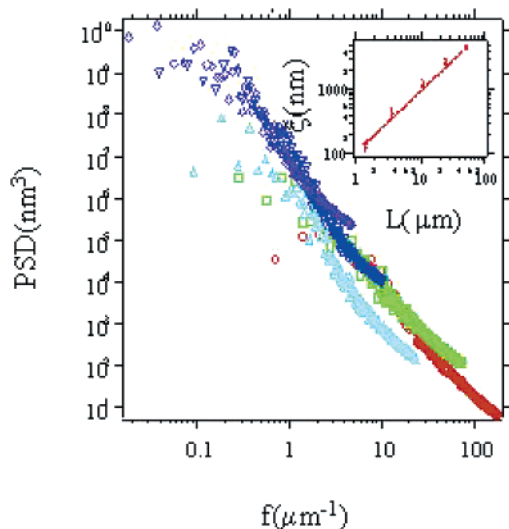
Figure 5. Power spectral density (PSD) of the topography from AFM images of different scan length: L (μm) = 54 (lower triangles), 24 (diamonds), 10 (upper triangles), 5 (squares), 1 (circles). Inset shows the estimated correlation length (viz., the inverse of the breakdown frequency separating power law decay from the apparent plateau) versus the scan length L. The continuous line is the power law fitting yielding $x \approx L^{0.95(\pm 0.03)}$.

of scaling behavior of the thin film morphology is termed self-affinity,[18] and it has been previously observed in T6[14] and other oligomer thin films[19] grown in out of equilibrium conditions.

To quantify the self-affinity, in Figure 5 we compare the power spectral densities (PSD) estimated from AFM images at different scan lengths. Details of the analysis have been described in earlier works.[14b] PSD contains the information about the roughness, viz., the height fluctuations, and how this is correlated in space. It appears that for each scan length fluctuations are spatially correlated (power law decaying region vs spatial frequency) at high frequency. This extended power law decay is a fingerprint of self-affinity. On the other hand, the uncorrelated "white" spectrum (plateau) at low frequencies spans a few points, suggesting that the breakdown of correlations can be mainly ascribed to the finite AFM image size. This is confirmed in the inset, showing that the estimated correlation length is linear with the scan length of the AFM image.[19] Cropping together the spectra reveals that, except for the few points of white spectra at each length scale, the power law decay spans across 3 orders of magnitude of the spatial frequencies, viz., the whole range explored by the atomic force microscope. From the similarity with the optical measurements in Figures 2 and 3, we can infer that such a behavior would propagate at length scales up to hundreds of micrometers.

On the striped regions, we observed terraces that are typical of layered thin films (Figure 6). The smallest step observed between adjacent terraces (Figure 6b,c) was 2.0 ± 0.2 nm, which is consistent with the expected height of a monolayer of T5 molecules (molecular length: 2.2 nm) oriented almost normal with respect to the substrate.

III. X-ray Diffraction. The XRD profile of a T5 powder sample is reported in Figure 7a. The comparison with the pattern reported by Porzio et al.[7] indicates that the same unique crystalline phase is obtained. Also, the unit cell parameters (a

(18) Barabási, A. L.; Stanley, H. E. *Fractal Concepts in Surface Growth*; Cambridge University Press: Cambridge, UK, 1996.
(19) Tsamouras, D.; Palasantzas, G. *Appl. Phys. Lett.* **2002**, *80*, 4528−4530.
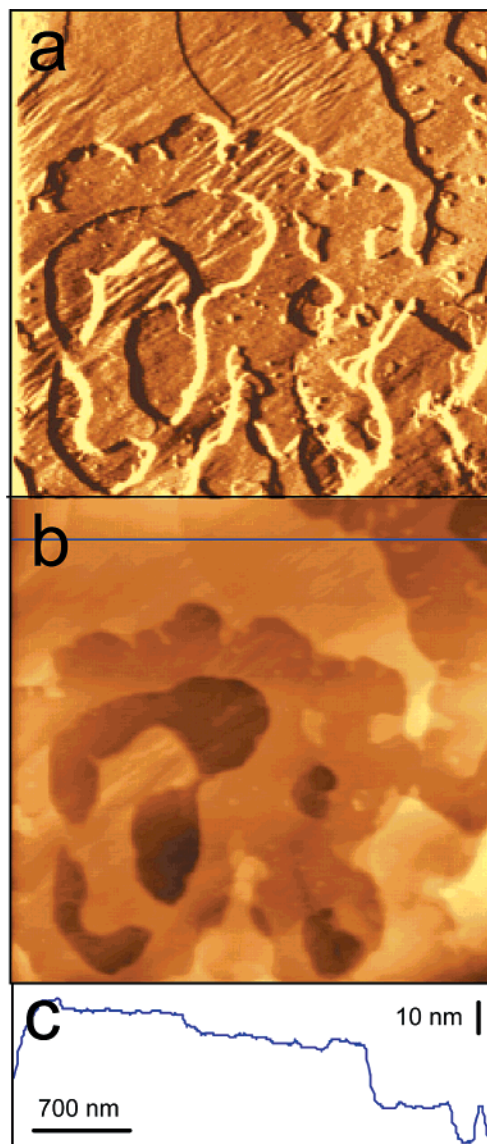
Figure 6. Layered morphology on top of striped domains: (a) AFM error signal image resolving the striped morphology at small length scales; (b) corresponding AFM topography showing the terraces. Height range z: 0−67 nm. (c) Profile along the solid line shown in (b); the smallest terrace step is 2.0 ± 0.2 nm which is consistent with a T5 molecule standing upright with respect to the surface plane.

= 3.91(1) nm, b = 0.780(2) nm, c = 0.597(4) nm, β = 98.5(8)°) are in good agreement with literature data.[7]

Figure 7b shows the XRD profile of a vacuum-evaporated thin film about 100 nm thick. The same angular position of the reflections indicates that both film and powders exhibit the same crystalline phase. A general decrease of reflection broadening is observed from powder to film, indicating the increase of the coherence length in the latter. Furthermore, in the vacuum-evaporated sample, the intensity increase of the $h00$ reflections supports the AFM observation of the terraced structure with a preferential orientation of these planes parallel to the glass support (substrate).

A further reduction of the peak widths and a reinforcing of the $h00$ reflections is detectable in the pattern of the melt-quenched sample, as shown in Figure 7c. Furthermore, numerous high-order $h00$ reflections become detectable, while the intensity of reflection (-411) ($2\theta = 20.0°$) is almost zero.
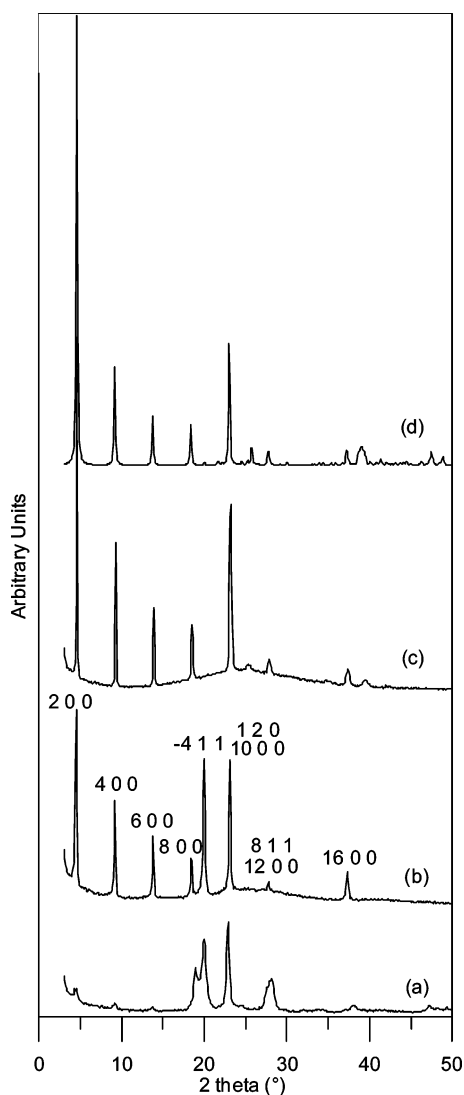
Figure 7. XRD profile of T5: (a) powder, (b) vacuum-evaporated 100 nm thick film, (c) the same film as (b) after melting−quenching. (d) XRD profile simulation of the melt-quenched film in (c).

The simulation of an X-ray diffraction profile employing a strong preferred orientation parameter along the ⟨100⟩ direction is reported in Figure 7d. From comparison of the simulated profile with that of the melt-quenched sample (Figure 7c), it is evident that the variation intensities of the reflections should be ascribed to an ordering process. This allows us to conclude that the sublimation step followed by melt quenching results in highly organized films.

In Figure 8, some sketches of the structure of the T5 layer on glass are proposed. The (100) plane (*b*,*c* plane) is positioned in contact with the glass surface to match X-ray results. As a consequence, the long axis of the T5 molecules is inclined by about 65° with respect to the glass surface, as can be seen in Figure 8b where the projection on the *a*,*c* plane is reported. Figure 8c shows the projection obtained when rotating the previous view by 90° with respect to an axis perpendicular to the substrate surface. The molecules appear grouped along parallel columns.

The line broadening of the (400) reflection was used to evaluate the length D_{hkl} of the coherent domains in the crystal. D_{hkl} values were calculated from the widths at half-maximum

$\beta_{1/2}$, in the hypothesis of negligible strain, using the Scherrer equation: $D_{hkl} K\lambda/\beta_{1/2} \cos \theta$, where λ is the wavelength, θ is the diffraction angle, and K is a constant depending on crystal habit (chosen as 1.0).[20] The instrumental broadening was taken into proper account.

The D_{hkl} values calculated for the powder, the sublimed, and the melt-quenched samples are, respectively, 28 ± 5, 45 ± 5, 80 ± 10 nm, showing that the length of coherent domains increases after repeated treatments.

IV. FET Mobility Measurements. A thin film field-effect device with the bottom-contact configuration was used to measure the charge carrier mobility of T5 (Figure 9a). T5 film was grown by vacuum sublimation on the gate insulator and the source and drain metal electrodes.

To improve the electrical performance of T5 films, different film thicknesses and substrate temperatures were tested. The best electrical behavior was obtained for 20 nm film thickness, while changing the substrate temperature between 30 and 60 °C did not introduce any significant improvement.

In Figure 9b, a typical plot of drain current I_D versus drain voltage V_D at various gate voltages V_G is reported for a 20 nm T5 film evaporated on 350 nm thermally grown SiO_2 as the gate insulator and a 100 nm gold source and drain electrodes. The heavily doped n-type Si wafer acts as a gate for the FET devices. As expected, the channel current increases as the voltage becomes more negative, indicating that the carriers are positive charges (holes). In Figure 9c, left axis, the transfer characteristic for the same device operating in the saturation region ($-V_D > V_G - V_T$, where V_T is the FET threshold voltage) is reported.

The charge carrier mobility of T5 calculated in the FET saturation regime is obtained from the slope of the plot of $|I_D|^{1/2}$ versus V_G (Figure 9c, right axis) and is 0.02 cm²/(V·s) at room temperature. The current modulation, usually referred to as the I_{ON}/I_{OFF} ratio, is around 5×10^5 when V_G is scanned from -100 to 20 V and V_D is held constant at -100 V, while it reduces to 10^3 when scanning the V_G voltage from -100 to 0 V, mantaining V_D at -100 V. This reduction is due to the high carrier concentration in the channel region related to the very large drain polarization used.

Discussion

Our data demonstrate that the crystalline order of T5 films is greater − although of the same type − than that displayed by the even members of the unsubstituted oligothiophene homologous series.

XRD shows that T5 thin films consist of layered structures in a monoclinic arrangement, with nearly planar molecules standing on the substrate with the long molecular axes tilted by about 65° with respect to the substrate plane. This type of organization, with the molecules standing upright to the surface of the substrate, is similar to that observed for vacuum-evaporated sexithiophene or its α,ω-dihexyl-substituted derivative and is favorable to achieve in-plane high charge carrier mobilities.[2e,8]

In thin films of T5, domains are grown with their (*b*,*c*) face parallel to the substrate and with the molecules piled up side-

(20) Alexander, L. E. *X-ray Diffraction Methods in Polymer Science*; Wiley-Interscience: New York, 1969.
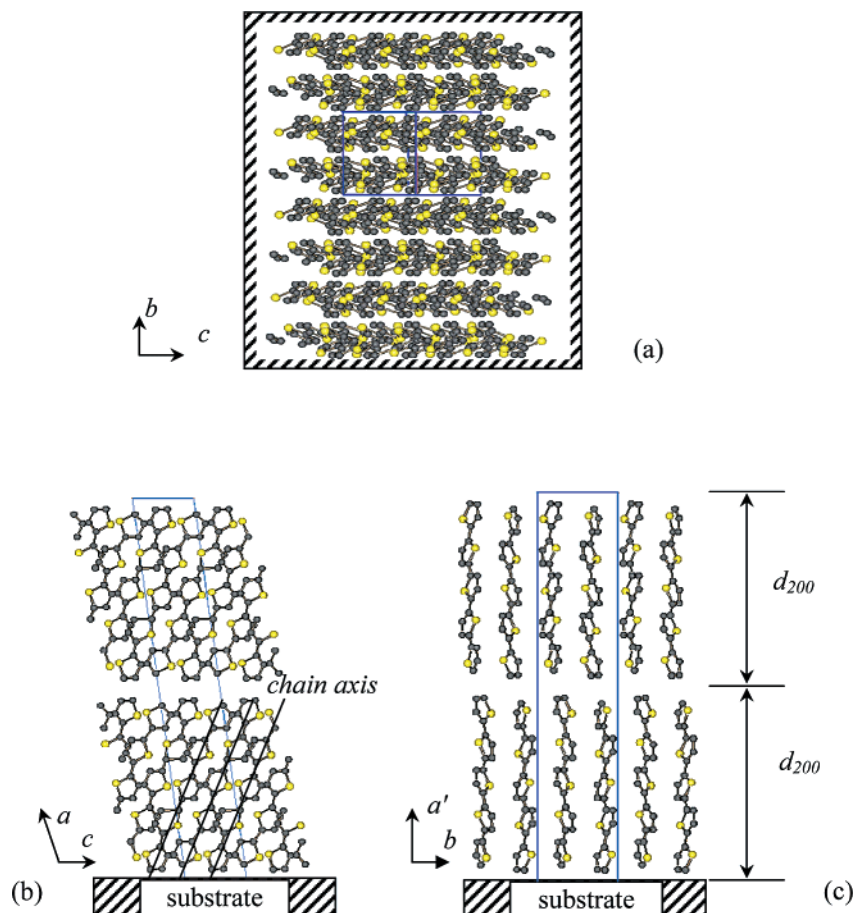
Figure 8. Sketches of the organization of T5 molecules on the glass substrate after melting−quenching: (a) projection on the glass plane, (b) projection on the (a,c) plane, (c) projection on the (a′,c) plane (a′ = a sin β).
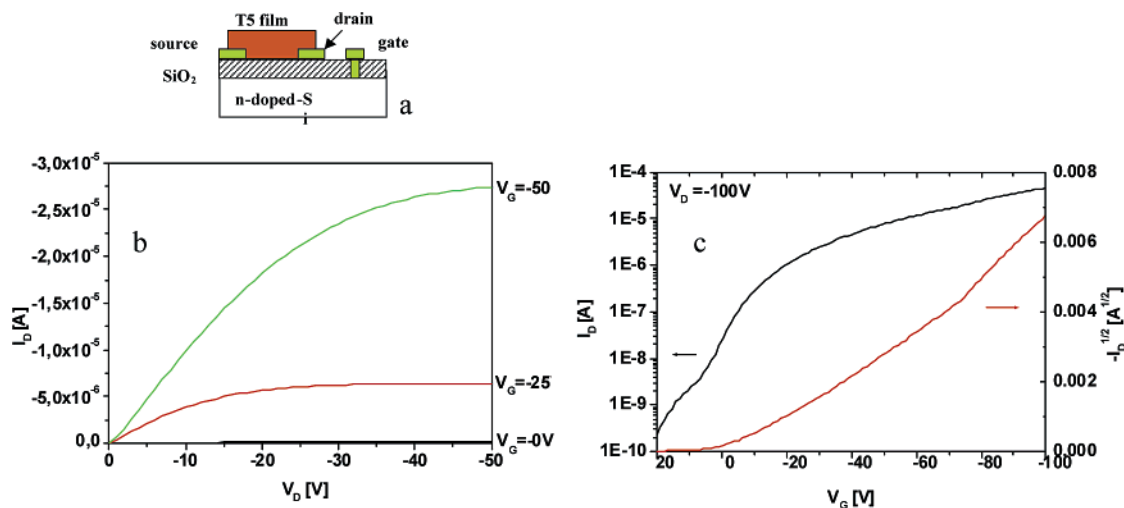

Figure 9. (a) Bottom-contact configuration of the TFT device. (b) Plot of the drain current I_D characteristic versus drain voltage V_D at different gate voltages (V_G). (c) Semilogarithmic plot of I_D versus V_G (left y axis) and plot of $I_D^{1/2}$ (right axis).

by-side along parallel columns. Heating the film up to the melting temperature followed by rapid thermal quenching enhances the molecular ordering and increases the dimension of coherent crystalline domains, as demonstrated by the disappearance of the (−411) reflection and the enhancement/sharpening of h00 reflections. Polarized microscopy shows that the melting−quenching process causes the formation of strongly birefringent single-crystal-like islands of micrometer size, exhibiting parallel stripes on the surface.

The morphological picture of the crystal domains offered by atomic force microscopy is consistent with the structural model developed from X-ray diffraction data. AFM shows the presence of stacked terraces, which are integer multiples of layers 2.0 ± 0.2 nm thick. This is in agreement with an arrangement of the crystal unit cell with the basal (100) plane in contact with the substrate. In this situation, a molecular layer fills the space between (200) planes which are separated by a distance of 2.0 nm. Moreover, AFM shows the existence of a recurring motif

based on aligned stripes from the scale of nanometers up to the length scales of the whole crystal in the submillimeter range.

The remarkable result is that the striped morphology of the crystalline islands formed by melt-quenching of T5 is preserved and amplified at a length scale across 3−4 orders of magnitude. In nature, 1−1.5 orders of magnitude are commonly observed; 2 orders represent an uncommon observation.[19] Self-affinity across more than 3 orders represents a behavior rarely observed.[21] This implies that in T5 films, spatial fluctuations, which represent the deviation from a perfectly ordered arrangement, are not random. T5 exhibits a hierarchical architecture of striped domains, from the nanometer scale-up to several millimeters, built by reiteration across multiple length scales of the same building block. The morphology in Figures 2−6 together with the XRD evidence suggests that such a building block may be an anisotropic tiny slab or fibril made of a few molecules. In this case, we can completely rule out anisotropy induced by the substrate. The fractures observed by AFM, which are parallel or perpendicular to the direction of the stripes, can be ascribed to cleavage planes corresponding to the (*a,b*) and (*b,c*) molecular planes, but the spatial correlation is retained across them. As a term of comparison, T6 thin films exhibit a self-affinity behavior[14] across 1−2 orders of magnitude of the spatial length scales, and with the coexistence of different morphologies at different length scales due to the presence of length scale dependent energy barriers or growth mechanisms.[22,23]

The pioneering work of Garnier and co-workers[2e] has demonstrated that high conjugation along the long molecular axis and close packing along at least one of the small molecular axis are requisites for high charge mobility. However, the role of long range spatial correlations has been marginally explored. For T5 thin films, we measured a FET hole mobility of 0.02 cm^2/(V·s), obtained without any treatment of the SiO$_2$/Si substrate (held at room temperature during deposition). This value is the highest reported so far for T5[16] and is comparable to the best FET mobilities in T6 thin films.[4] The high charge carrier mobility measured for T5 may be a consequence of its highly ordered crystalline structure together with its hierarchical organization that spans all length scales relevant to FET transport, viz., from the molecular scales up to the channel length. The large I_{ON}/I_{OFF} current ratio achieved (5×10^5) is consistent with the high purity of the T5 samples used in this study and indicates the effectiveness of the preparation and purification methodologies employed here.

We believe that excellent layers for charge transport could be obtained by controlling the construction of the hierarchical organization of T5 onto a device structure. In fact, experimental evidence indicates that charge carrier mobility increases with correlation lengths and depends critically on the extent of domain boundaries.[4] In the case of T5 melt-quenched films, we would expect an enhancement of the mobility, because T5 correlation length would match the relevant length scale of the transistor, viz., channel length, and hence carriers would be generated and transported across a single domain. Casting of highly ordered and oriented domains into transistors is currently in progress.

(21) Krim, J.; Palasantzas, G. *Int. J. Mod. Phys.* **1995**, *9*, 599−632.
(22) Biscarini, F. Scanning Force Microscopy of Conjugated Oligomer Thin Films Grown in High-Vacuum. In *Scanning Probe Microscopy of Polymers*; Ratner, B. B., Tsukruk, V. V., Eds.; ACS Book: Washington DC, 1998; p 163.
(23) Moretti, P. Tesi di Laurea; Università di Bologna, 1998.

Conclusion

We have shown that in T5 films a unique combination of molecular order and self-affine morphology is achieved, resulting in a self-organized hierarchical architecture across 3−4 orders of magnitudes of the spatial length scales. Such a behavior has not been observed to this extent in any other organic semiconductor. Self-affinity across multiple length scales can become extremely desirable for charge transport because it would enable matching the correlation length of the active layer with the channel length in any FET devices. In this way, transistors would operate with single domains or highly correlated transport layers, improving their charge mobility and other relevant properties such as stress and modulation. From the fabrication point of view, the self-affine organization of T5 into a transistor layout could be exploited for obtaining high performance devices without the need of high-resolution down scaling of the device layout, which would be desirable in view of sustainable electronics production.

Experimental Section

Material. The synthesis of T5 was carried out according to the modalities described in ref 6f, by solvent-free, microwave assisted coupling of α,ω-dibromo-2,2′:5′,2″-terthiophene with 2-thienyl boronic acid (Suzuki coupling) in the presence of palladium catalysts. T5 was first crystallized from dioxane−water, and then sublimed under vacuum using a coldfinger. The melting point of the sublimed material was 256 °C. Proton NMR, mass spectrometry, and TGA plot data of sublimed T5 are reported as Supporting Information. Thin films of T5 were deposited by vacuum evaporation (1×10^{-6} mbar) at a rate of about 0.1 nm/s. Film thickness was measured using a quartz microbalance. DSC measurements were performed with a TA Instruments DSC-2010 apparatus, using heating rates of 10 and 2 °C/min. The temperature scale was calibrated with high purity standards. The melting of the samples, either powders or films, was obtained using the heating plate of a Leica DMLS optical microscope.

Atomic Force Microscopy. AFM was performed in noncontact mode, using a CP-Multimode Head by Thermo Microscope (Santa Clara, CA) with a linearized scanner with a 90 μm scan length, and a standalone AFM (MDT Moscow). Images were rotated to make the fibrils stretching from top to bottom, then corrected line-by-line for background trend effects by removal of the second-order polynomial fitting. Fourier analysis was carried out ex situ with image analysis software, and analysis of the PSD spectra along the direction perpendicular to the fibrils was carried out with Igor Pro 4.0.

X-ray Diffraction. XRD measurements were carried out at room temperature with a Bragg/Brentano diffractometer (Philips PW1050/ 61-PW1710), equipped with a graphite monochromator in the diffracted beam, using Cu anode as the X-ray source. Data were collected in the 2θ range 3−60° counting for 5 s at each 0.1° step. The simulated X-ray diffraction pattern was obtained by using the PowderCell program.[24]

FET Device Fabrication. Heavily doped silicon single-crystal wafers were used as substrates, and a layer of 350 nm of SiO$_2$ (grown by thermal oxidation) was used as the gate dielectric. Au (80 nm) was successively evaporated and photolithographically delineated to obtain the gate and the source and drain electrodes. The interdigitated structure of the source−drain contacts determined a channel width of 1.1 cm and a channel length of 10 μm. On every test pattern, a thin layer (20− 50 nm thick) of the oligomer was deposited on the channel region (through a metal mask) by vacuum evaporation (1×10^{-6} mbar) at a

(24) Kraus, W.; Nolze, G. PowderCell for Windows, version 2.3.

rate of about 0.1 nm/s. The measurements were performed using a computer controlled parametric characterization system.

Supporting Information Available: Proton NMR, mass spectrum, TGA plot, and movie of T5 crystalline islands exctinction. This material is available free of charge via the Internet at http://pubs.acs.org.

JA036152M